PATTERNS & PHENOTYPES

Beyond the Closed Suture in Apert Syndrome Mouse Models: Evidence of Primary Effects of FGFR2 Signaling on Facial Shape at Birth

Neus Martínez-Abadías,[1] Christopher Percival,[1] Kristina Aldridge,[2] Cheryl A. Hill,[2] Timothy Ryan,[1] Satama Sirivunnabood,[1] Yingli Wang,[3] Ethylin Wang Jabs,[3] and Joan T. Richtsmeier[1]*

Apert syndrome is a congenital disorder caused mainly by two neighboring mutations on fibroblast growth factor receptor 2 (FGFR2). Premature closure of the coronal suture is commonly considered the identifying and primary defect triggering or preceding the additional cranial malformations of Apert phenotype. Here we use two transgenic mouse models of Apert syndrome, $Fgfr2^{+/S252W}$ and $Fgfr2^{+/P253R}$, to explore variation in cranial phenotypes in newborn (P0) mice. Results show that the facial skeleton is the most affected region of the cranium. Coronal suture patency shows marked variation that is not strongly correlated with skull dysmorphology. The craniofacial effects of the FGFR2 mutations are similar, but $Fgfr2^{+/S252W}$ mutant mice display significantly more severe dysmorphology localized to the posterior palate. Our results demonstrate that coronal suture closure is neither the primary nor the sole locus of skull dysmorphology in these mouse models for Apert syndrome, but that the face is also primarily affected. *Developmental Dynamics 239:3058–3071, 2010.* © 2010 Wiley-Liss, Inc.

Key words: Apert syndrome; craniofacial shape; craniosynostosis; FGFR2; mouse model; suture

Accepted 5 August 2010

INTRODUCTION

Apert syndrome is a congenital autosomal dominant disorder characterized by cranial, neural, limb, and visceral malformations [MIM 101200], with disease prevalence of 15–16 per million live births (Cohen et al., 1992). Individuals with Apert syndrome present a complex and variable craniofacial phenotype with premature fusion of the coronal suture (craniosynostosis), a large defect of the anterior fontanelle, brachycephaly, midfacial retrusion, maxillary hypo-plasia, ocular hypertelorism, and proptosis (Cohen, 2000). Almost 99% of reported cases of Apert syndrome carry one of two mutations in the highly conserved linker region connecting the second and third extracellular immunoglobulin-like domains of fibroblast growth factor receptor 2 (FGFR2) (Park et al., 1995a; 1995b; Wilkie et al., 1995). Each of these gain-of-function mutations (Ser252Trp and Pro253Arg) are missense substitutions involving adjacent amino acids that alter the ligand-binding affinity and specificity of the receptors that can, as a result, be activated inap-propriately (Plotnikov et al., 2000; Ibrahimi et al., 2001; Yu and Ornitz, 2001; Yu et al., 2003). As a consequence, many processes in osteogenic cells mediated by the FGF/FGFR signaling pathway (e.g., patterns of cell proliferation, differentiation, migration, adhesion, and death) (Ornitz and Marie, 2002; Hajihosseini, 2008; Marie et al., 2008), as well as those involved in the development of other tissues, are potentially affected (Ford-Perriss et al., 2001; Inatani et al., 2003; Schul-ler et al., 2008; Turner and Grose,

2010). Approximately 67% of individuals with Apert syndrome have a dominant FGFR2 S252W mutation, while the remaining 33% have a dominant FGFR2 P253R mutation (Wilkie et al., 1995; von Gernet et al., 2000).

Despite the limited mutational spectrum responsible for Apert syndrome (Slaney et al., 1996), the phenotypic outcome of these two genetic changes is neither consistent nor localized to a particular bodily system. There is no simple one-to-one correspondence between genotype and phenotype, and dysmorphologies of development are pervasive. Analysis of individuals with Apert syndrome reveals variation in the effects across tissues and variation in the severity of these effects (Cunningham et al., 2007). Interestingly, other FGFR1, -2, and -3 related craniosynostosis syndromes, such as Crouzon, Pfeiffer, Jackson-Weiss, Muenke, and Saethre-Chotzen syndromes, present overlapping craniofacial phenotypes prompting the hypothesis that these syndromes represent a phenotypic clinical spectrum of related genetic disorders that can be produced by different combinations of mutations in genes working in similar signaling cascades (Cunningham et al., 2007). The precise genetic and developmental bases of craniofacial variation in these syndromes are not fully understood.

Craniosynostosis, the premature closure of cranial sutures, is the common denominator in FGFR1, -2, and -3 related craniosynostosis syndromes. As the most frequent, salient, and clinically manageable feature, much of the clinical, molecular, and morphological research has focused on the cranial vault sutures and the mechanisms underlying suture patency and closure (Cunningham et al., 2007). As a result, premature suture closure is often considered, explicitly or implicitly, the primary anomaly and contributory to skull dysmorphology in craniosynostosis syndromes (Cohen, 1986, 1993). Additional neurocranial and facial traits that together define the complex craniofacial phenotype associated with these craniosynostosis syndromes have often not been given the same relevance and have been considered secondary to calvarial suture fusion (Cohen,

1986, 1993; Cohen and Kreiborg, 1996). Craniofacial dysmorphogenesis is, however, a complex process in these syndromes, involving a potentially broad influence of mutated genes in the hierarchies of various networks that impact dynamic patterns of gene expression and regulation, aspects of cell signaling, developmental interactions among emergent properties of tissues, as well as continuously changing biomechanical forces acting at different times of growth and development.

Given its relatively low prevalence, studies of humans may never provide data adequate to illuminate the genotype-phenotype continuum in Apert syndrome. Consequently, the study of mouse models becomes critical to understanding variation in Apert syndrome phenotypes. The correspondence between Apert syndrome transgenic mouse models and human patients with Apert syndrome has been demonstrated at the molecular, histological, and morphological levels (Chen et al., 2003; Wang et al., 2005, 2010; Holmes et al., 2009; Aldridge et al., 2010; Du et al., 2010). Here, we quantify skull shape variation in Apert syndrome using the Apert syndrome $Fgfr2^{+/S252W}$ and $Fgfr2^{+/P253R}$ mouse models, generated on the same C57BL/6J genetic background (Wang et al., 2005, 2010). Morphometric analysis of three-dimensional (3D) landmark data precisely recorded from high-resolution micro-computed tomography (μCT) images of the skulls of newborn (P0) mice enables estimation of morphological variation within and among groups and detection of localized shape differences resulting from phenogenetic processes that contribute to Apert syndrome craniofacial phenotypes.

Adopting well-used evolutionary models that partition the skull into cranial vault, cranial base, and facial skeleton (Cheverud, 1995; Richtsmeier, 2002; Sperber et al., 2010), we statistically estimate the severity of localized dysmorphology across these components of the murine skull at P0. The underlying assumption is that the shape configuration providing the best differentiation between mutant and non-mutant mice in both transgenic lines will reflect main and direct morphological effects of the Apert

syndrome FGFR2 mutations. As samples of different ages are not included in this study, our analyses do not test causality or the temporal sequence of the appearance of traits defining the Apert phenotype. Our goals are to: (1) quantitatively evaluate global and local morphological differences among and within groups and identify the cranial region(s) that is(are) most affected at this early stage of development, and (2) determine the relationship between coronal suture patency and skull dysmorphology. Since coronal suture closure is considered a main effect of these FGFR2 mutations, we expect that the cranial vault will provide the best separation between groups and that suture patency will be highly correlated with the skull dysmorphology associated with Apert syndrome.

RESULTS

Skull phenotypes: Comparisons of Apert Syndrome $Fgfr2^{+/S252W}$ and $Fgfr2^{+/P253R}$ Mouse Models

We compared phenotypic variation of P0 skulls of $Fgfr2^{+/S252W}$ and $Fgfr2^{+/P253R}$ mice and their non-mutant littermates (Table 1) using various morphometric methods that allow us to characterize overall variation and pinpoint highly localized shape differences among groups. Three-dimensional coordinates of 51 cranial landmarks (see Supp. Fig. S1 and Supp. Table S1, which are available online, and http://getahead.psu.edu/LandmarkNewVersion/P0mouseskull_updated_applet.html) were recorded on the 3D μCT isosurfaces reconstructed using two software packages for the visualization of medical images, Avizo 6.0 (Visualization Sciences Group, VSG) and eTDIPS (http://www.cc.nih.gov/cip/software/etdips/). We defined subsets of 3D landmarks to represent the shape of the global skull as well as the shape of the three major regions of the mammalian skull: face, cranial vault, and cranial base (Supp. Fig. S1 and Supp. Table S1). For all four datasets, we first performed a General Procrustes analysis to superimpose the coordinate data and to extract shape

TABLE 1. Sample Sizes (and Corresponding Percentages) in Apert Syndrome *Fgfr2*$^{+/S252W}$ and *Fgfr2*$^{+/P253R}$ Mutant Mice and Their Non-Mutant Littermates at P0[a]

Genotype	N	Coronal suture					Zygomatic-maxillary		Premaxilla-maxillary	
		OPEN	BICOR	PART	RUNIC	LUNIC	Open	Fused	Open	Fused
+/+	19	18 (95%)	-	1 (5%)	-	-	19 (100%)	-	19 (100%)	-
+/**S252W**	16	-	11 (69%)	4 (25%)	-	1 (6%)	-	16(100%)	-	16(100%)
+/+	12	10 (84%)	-	1 (8%)	-	1 (8%)	12 (100%)	-	12 (100%)	-
+/**P253R**	26	-	13 (50%)	9 (35%)	3 (11%)	1 (4%)	-	26(100%)	-	26(100%)

[a]For each group, qualitative scores on suture patency (open, partial, fused) are provided. OPEN: No closure or overlap visualized at either side of the coronal suture (both sides scored as open, O); BICOR: Bicoronal synostosis (almost no open areas visualized on either right or left side, right and left scored as fused, F); PART: Partial (one or two sides scored as partial, P); RUNIC: Right unicoronal (right side showing almost complete overlapping/fusion of bony fronts and scored as fused, while left side is open and scored as open); LUNIC: Left unicoronal (left side scored as fused and right as open). For exact definitions of patency states (O, P, F), see Experimental Procedures section.

information (Rohlf and Slice, 1990; Dryden and Mardia, 1998). This procedure minimizes the influence of size and adopts a single orientation for all specimens by shifting the landmark configurations to a common position, scaling them to a standard size and rotating them until a best fit of corresponding landmarks is achieved. We then analyzed shape variation using Principal Component Analysis (PCA), a data exploration technique that performs an orthogonal decomposition of the data and transforms the resulting Procrustes coordinates into a smaller number of uncorrelated variables called principal components (PCs). Individuals are scored on each PC so that a distribution of the individuals can be plotted along these axes. The first PC (PC1) accounts for the largest amount of variation in the data, and the second PC (PC2) accounts for the second largest amount of variation, and so on (Reyment et al., 1984).

Global Skull Shape Analysis: Similarities in Craniofacial Shape Among Apert Mouse Models

The PCA analysis based on the Procrustes coordinates of the subset of 39 landmarks that define the global skull configuration and sample information from the entire skull (Supp. Table S1) shows a clear separation between Apert syndrome *Fgfr2*$^{+/S252W}$ and *Fgfr2*$^{+/P253R}$ mutant mice and their non-mutant littermates along PC1, which accounts for more than 52% of the total shape variation (Fig. 1A).

Apert syndrome *Fgfr2*$^{+/S252W}$ and *Fgfr2*$^{+/P253R}$ mutant mice overlap along PC1 and PC2 showing a range of variation so extensive as to make the two groups indistinguishable. Non-mutant littermates show a more reduced range of variation along both axes but also completely overlap, indicating that they share similar skull morphologies. None of the remaining principal components separate any known groups (data not shown).

Procrustes superimposition reduces the effects of scale, but does not eliminate allometric shape variation that is related to size. We mathematically corrected for correlations among shape variables due to allometry (size-related differences in shape) by computing a regression of shape on centroid size following the methods of Drake and Klingenberg (2008) (see Experimental Procedures section for more details). The residual estimates for each specimen were used to compute another PCA that represents the distribution of our data after the effects of allometry are removed. The separation previously seen between mutant and non-mutant mice along PC1 is no longer apparent (Fig. 1B), indicating that the main difference between mice carrying either of the two FGFR2 mutations and non-mutant littermates is an allometric shape difference, one that is tied closely to differences in size. Non-mutant mice remain at the negative end of PC1, but there is substantial overlap among groups along this axis (Fig. 1B).

Shape differences between groups are displayed as wireframe deformations (Fig. 2) corresponding to extreme positive and negative values of the PC1

shown in Figure 1B. Mice carrying either the *Fgfr2*$^{+/S252W}$ or the *Fgfr2*$^{+/P253R}$ mutation (represented by the negative extreme of PC1, orange wireframe) show the typical brachycephalic shape of Apert syndrome phenotype, with wider cranial vaults at the parietal and temporal levels than the mean shape (grey dashed wireframe). In comparison to non-mutant littermates (located on the positive extreme of PC1, blue wireframe), *Fgfr2*$^{+/S252W}$ and *Fgfr2*$^{+/P253R}$ mutant mice also show midfacial hypoplasia, represented by more posterior placement of facial and palatal landmarks. The cranial base is inferiorly displaced in mutant mice, and the region of the skull where the cranial base joins the face is oriented differently in the two groups, being more flexed in the mutant groups.

Regional Skull Shape Analysis: Localized Differences in Craniofacial Shape Among Apert Mouse Models

We explored regional shape variation by performing separate General Procrustes and PCA analyses using three different configurations of 3D landmark coordinates (Supp. Fig. S1 and Supp. Table S1) representing the facial skeleton (19 landmarks), the cranial base (14 landmarks), and the cranial vault (6 landmarks) after removing the effects of allometry.

The PCA shape analysis of the cranial vault shows limited separation of *Fgfr2*$^{+/S252W}$ and *Fgfr2*$^{+/P253R}$ mutant mice from the non-mutant littermates,
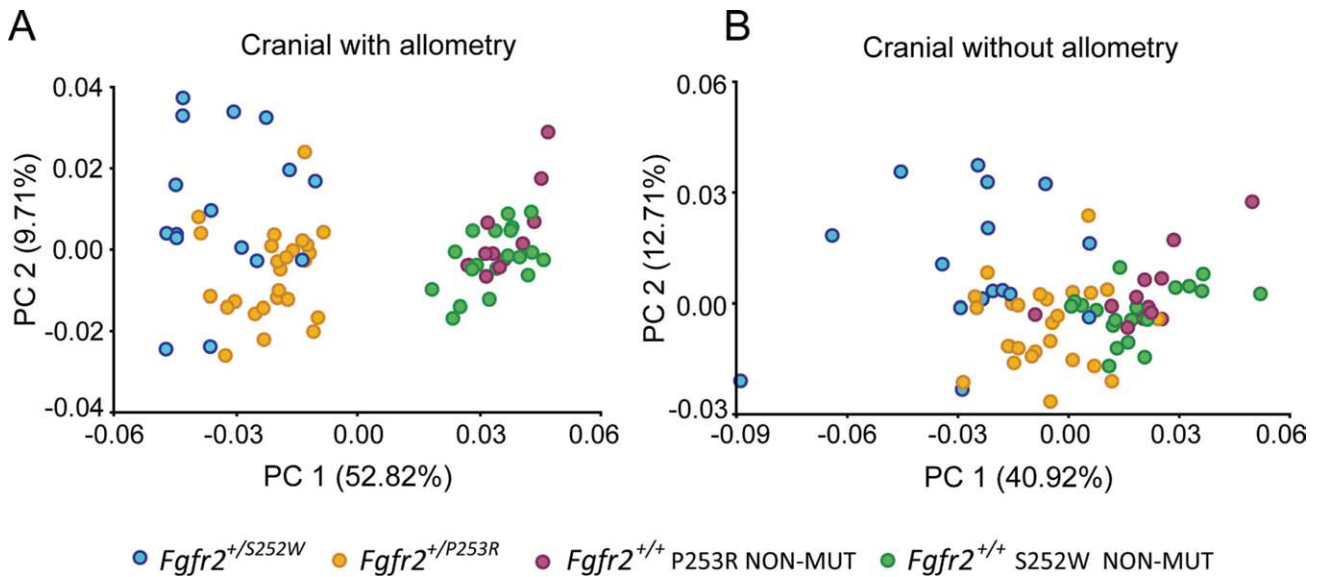
Fig. 1. Results of PCA analyses based on Procrustes coordinates of a global skull configuration of landmarks. Scatter plots of PC1 and PC2 scores before (**A**) and after adjusting for the effects of allometry (**B**).
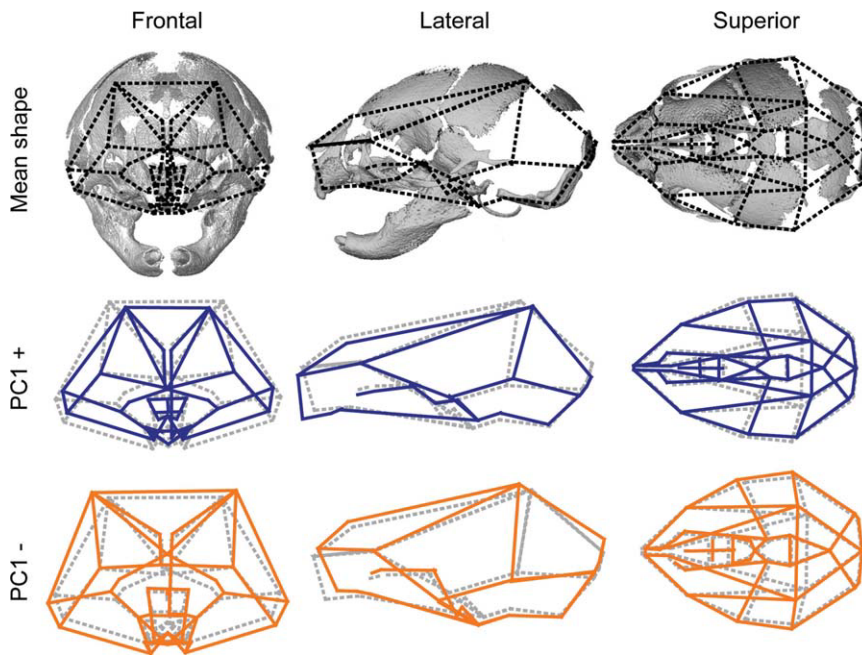
Fig. 2. Wireframes displaying skull morphologies along PC1 of the PCA analysis based on the global skull configuration of landmarks. **Top:** Mean shapes along PC1 are superimposed on a frontal, lateral, and superior view of the skull of a non-mutant mouse to provide an anatomical reference for interpretation. **Middle:** Blue wireframes represent the morphology associated with the specimens located on the positive extreme of PC1 (non-mutant littermates) in comparison to the mean shape of the sample (grey dashed wireframe). **Bottom:** Orange wireframes represent the morphology associated with the specimens located on the negative extreme of PC1 ($Fgfr2^{+/S252W}$ and $Fgfr2^{+/P253R}$ mutant mice) in comparison to the mean shape of the sample (grey dashed wireframe).

but specimens from all groups overlap along the two first PCs (Fig. 3A). Within the positive side of PC1, only $Fgfr2^{+/P253R}$ mice overlap with non-mutant littermates, whereas $Fgfr2^{+/S252W}$ mice are positioned along the negative side of PC1 and occupy the most extreme positions. The PCA shape analysis of the cranial base separates $Fgfr2^{+/S252W}$ and $Fgfr2^{+/P253R}$ mice from their non-mutant littermates, but there is considerable overlap among the two mutant groups (Fig. 3B). $Fgfr2^{+/S252W}$ mice occupy a larger area of the shape space indicating a larger range of variation for cranial base shape for this group, including an extreme outlier that overlaps with non-mutant mice along PC1. The PCA shape analysis of the facial skeleton separates $Fgfr2^{+/S252W}$ and $Fgfr2^{+/P253R}$ mice from their non-mutant littermates and shows clear separation between $Fgfr2^{+/S252W}$ and $Fgfr2^{+/P253R}$ mice on the combined basis of PC1 and PC2 (Fig. 3C), indicating significant differences in facial structure between the mutant specimens of the two Apert mouse models.

Analyses of linear distances using traditional methods of analysis and including data on suture patency further support these findings (see Supp. Fig. S2).

Face is the Most Affected Region in Apert Mutant Mice at P0

Given that our results suggest overall similarity, but localized shape differences that distinguish $Fgfr2^{+/S252W}$ and $Fgfr2^{+/P253R}$ Apert syndrome mouse models, we tested for statistically significant shape difference using Euclidean Distance Matrix Analysis (EDMA) (Lele and Richtsmeier, 2001) and the same subsets of landmarks that describe the cranial vault, the base, and the face (Supp. Fig. S1 and Supp. Table S1). EDMA (Lele and Richtsmeier, 2001) is a coordinate system-free approach that estimates differences in all possible pairs of inter-landmark distances and allows non-parametric
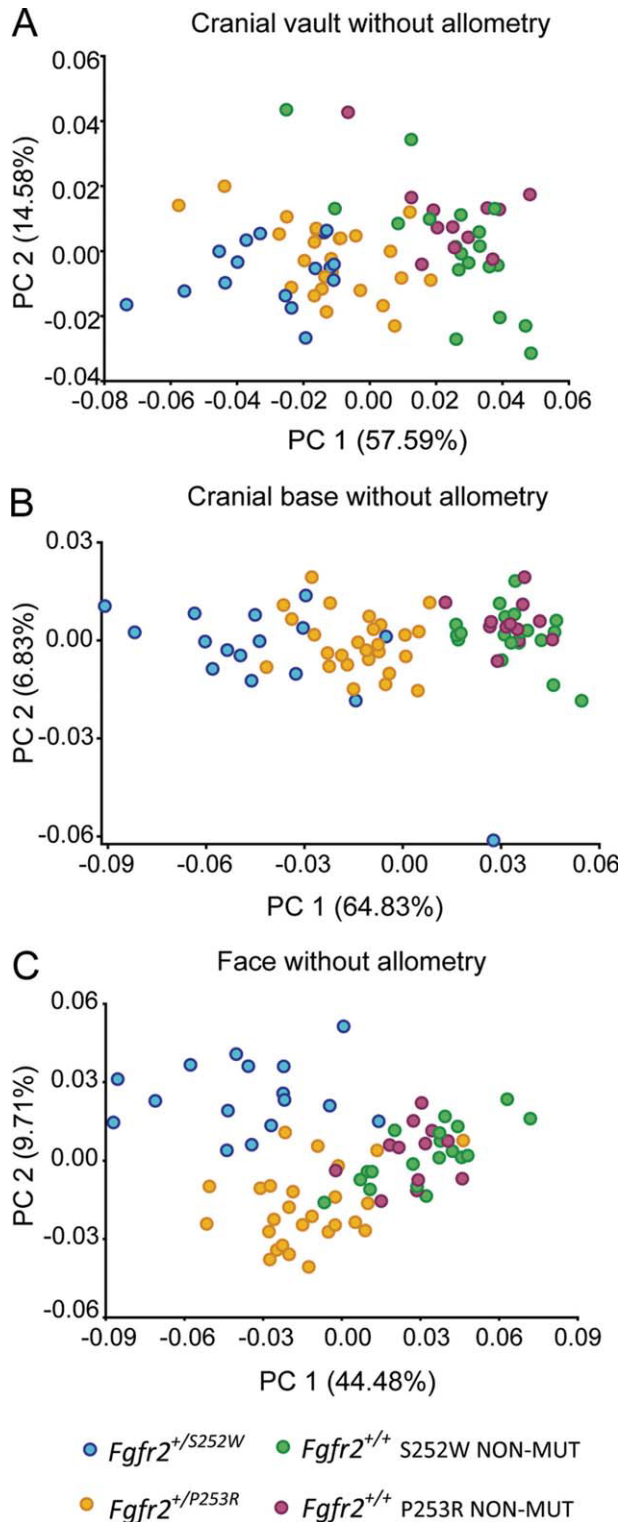
Fig. 3. Results of PCA analyses based on Procrustes coordinates of regional configuration of landmarks collected on the skull. Scatter plots of PC1 and PC2 scores of the cranial vault (**A**), the cranial base (**B**), and the face (**C**) after adjusting for the effects of allometry.

confidence interval estimation for statistical testing of the morphological differences between the groups.

EDMA demonstrated statistically significant differences in the facial skeleton, cranial base, and cranial vault between each mutant mouse model and their non-mutant littermates (Table 2). Moreover, a statistical comparison of the localized shape changes between each mutant group and its non-mutant littermates revealed similar effects of the two mutations on the cranial base and cranial vault, but a significant difference in the effects of each mutation on the facial skeleton. Confidence interval testing of the difference in the effects of the two mutations on the facial skeleton revealed that the main shape differences between $Fgfr2^{+/S252W}$ and $Fgfr2^{+/P253R}$ mice are concentrated on the posterior aspect of the palate (Fig. 4). In general, the magnitude of the differences between $Fgfr2^{+/S252W}$ mice and their non-mutant littermates are greater than the differences between $Fgfr2^{+/P253R}$ mice and their non-mutant littermates. However, these differences are not uniform (Fig. 4).

Patterns of Suture Patency

To compare the patterns of suture patency among $Fgfr2^{+/S252W}$ and $Fgfr2^{+/P253R}$ mice and their non-mutant littermates and to explore how synostosis is associated with Apert skull dysmorphologies at P0, we scored the patterns of suture patency as visualized on 3D µCT images in two facial sutures and the coronal sutures of the cranial vault.

Invariant Patterns of Facial Suture Patency

Qualitative scoring of suture patency of the zygomatic-maxillary and the premaxilla-maxillary sutures showed that these two facial sutures are consistently fused in $Fgfr2^{+/S252W}$ and $Fgfr2^{+/P253R}$ mutant mice at P0 but remain patent at P0 in non-mutant littermates (Table 1).

Highly Variable Patterns of Coronal Suture Patency

We scored the degree of patency on 3D µCT reconstructions of the coronal sutures using qualitative and quantitative approaches. We focus on the degree of suture patency rather than closure because the coronal suture is a beveled suture and the isosurface may not easily distinguish between overlapping suture fronts and fused sutures at the cellular level. However, the isosurface reliably differentiates those sections of the coronal suture that are completely open with the frontal and parietal fronts separated,
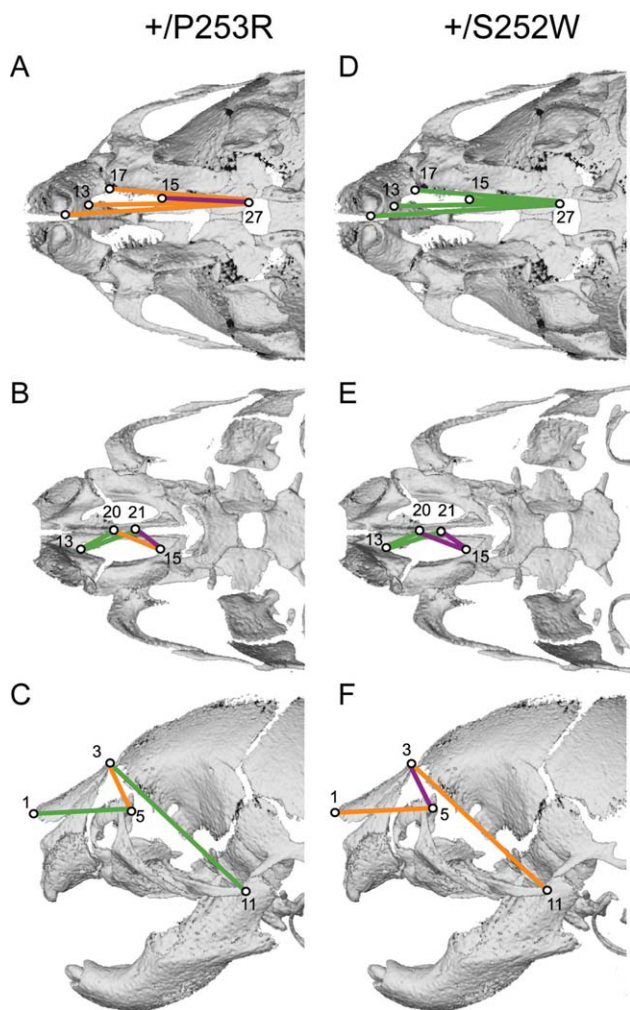
Fig. 4. EDMA results from comparisons of *Fgfr2*[+/P253R] and non-mutant littermates (left) and *Fgfr2*[+/S252W] and non-mutant littermates (right). From top to bottom: inferior view of palate (**A, D**), superior view of endocranium with vault removed (**B, E**), and lateral view (**C, F**) of a μCT 3D reconstruction of the P0 murine skull. Green lines indicate linear distances that are significantly shorter in mutants as compared to their non-mutant littermates; purple lines represent linear distances that are significantly longer in the mutants as compared to non-mutant littermates. Orange lines show linear distances that are similar in mutants and unaffected littermates (i.e., no statistical significant differences at the α = 0.1 level). Dimensions of the palate measuring the distance between the anterior and posterior turbinates and the palatine foramen (B, E) were the measures that were most affected (at least 10% longer/shorter in mutant mice in comparison to their non-mutant littermates). These analyses are limited to sagittal and left-sided landmarks to reduce the dimensionality of the data.

TABLE 2. EDMA Testing for Localized Differences in Shape Among *Fgfr2*[+/S252W] and *Fgfr2*[+/P253R] Mice and Their Non-Mutant Littermates at P0[a]

Comparison	Face (P)	Cranial base (P)	Cranial vault (P)
Fgfr2[+/S252W] vs *Fgfr2*^{+/+}	.001*	.01*	.001*
Fgfr2[+/P253R] vs *Fgfr2*^{+/+}	.001*	.006*	.047*
Fgfr2[+/S252W] vs *Fgfr2*[+/P253R]	.000*	.575	.068
S252W contrast vs P253R contrast	.004*	.176	.154

[a]S252W contrast versus P253R contrast refers to the statistical comparison of the differences defined between *Fgfr2*[+/S252W] mutant mice and non-mutant littermates with the differences defined between *Fgfr2*[+/P253R] mutant mice and non-mutant littermates. *Statistically significant comparisons (P < 0.05).

from those that are already fused or overlapping. These images represent a valuable snapshot of the dynamic process of suture development at P0, even if they do not enable prediction of future states of suture patency for individuals.

Initially we assigned a qualitative score of open, partially open, or fused (i.e., no open sections visualized) to the entire right and left coronal sutures of each mouse. This assessment revealed that, on at least one side, *Fgfr2*[+/S252W] and *Fgfr2*[+/P253R] mice always show some sections of the coronal suture that are not open (Table 1), though the extent and nature of this qualitative trait is highly variable across the sample. *Fgfr2*[+/S252W] and *Fgfr2*[+/P253R] mice classified using the traditional nomenclature of coronal synostosis range from complete bicoronal, to partial synostosis in one or both sutures, to complete unicoronal synostosis (in which one suture is completely open and the other shows almost no patency) (Fig. 5). *Fgfr2*[+/S252W] mice show a higher percentage of individuals with bicoronal suture closure (69%) and relatively fewer cases of partial and unicoronal synostosis (31%). In comparison, *Fgfr2*[+/P253R] mice show a lower percentage of individuals with bicoronal fusion (50%) and a higher frequency of partial and unicoronal synostosis (50%). Coronal sutures of non-mutant littermates are typically completely open (Table 1).

To more accurately estimate the variation observed in suture patency, we computed a quantitative measure of the degree of coronal suture patency as an index of the length of the suture that remains open divided by total suture length. Indices range from 1 (completely patent suture) to 0 (no aspects of the suture appear open, suture fronts are overlapping or fused). Intermediate values indicate varying magnitudes of suture patency. Figure 6 compares indices of right and left coronal patency in mutant and non-mutant mice of the two Apert mouse models. Non-mutant mice (NO-MUT) show indices close to 1 (i.e., patent sutures) and a narrow range of variation. Apert syndrome *Fgfr2*[+/S252W] and *Fgfr2*[+/P253R] mice (MUT) reveal a great deal of variation in the degree of patency of the right
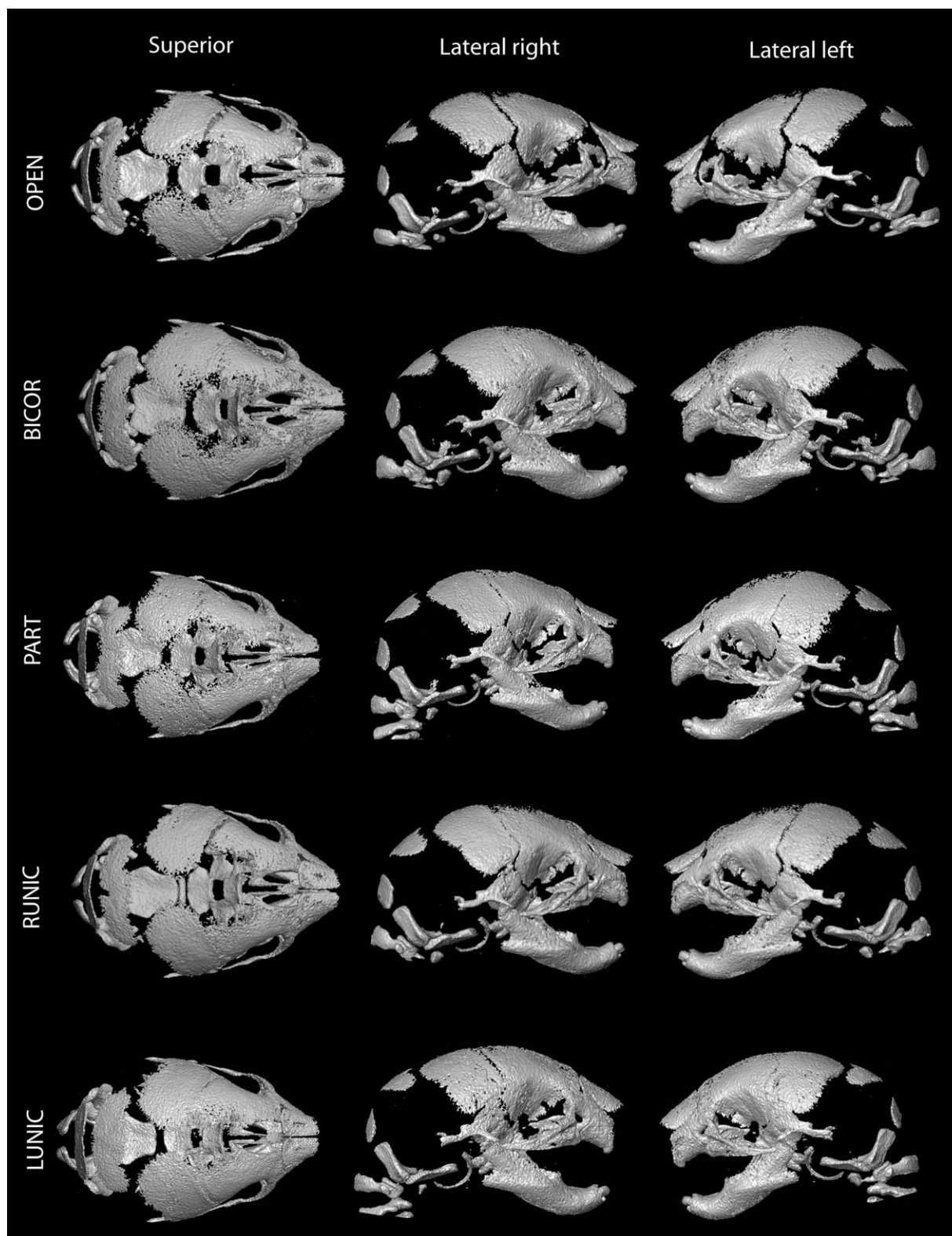
Developmental Dynamics

Fig. 5. Qualitative variation in suture patency in Apert mouse models. Superior, right and left lateral views of the 3D reconstructions of the skulls of five mice at P0. Row 1: non-mutant littermate of the S252W model with right and left patent coronal sutures (OPEN), row 2: $Fgfr2^{+/S252W}$ mutant mouse with bicoronal synostosis (BICOR), row 3: $Fgfr2^{+/S252W}$ mutant mouse with partial patency on either side of the coronal suture (PART), row 4: $Fgfr2^{+/P253R}$ mutant mouse with overlapping bone fronts at the right coronal suture and patent left coronal suture (RUNIC), and row 5: $Fgfr2^{+/S252W}$ mutant mouse with patent right coronal suture and not patent left coronal suture (LUNIC).
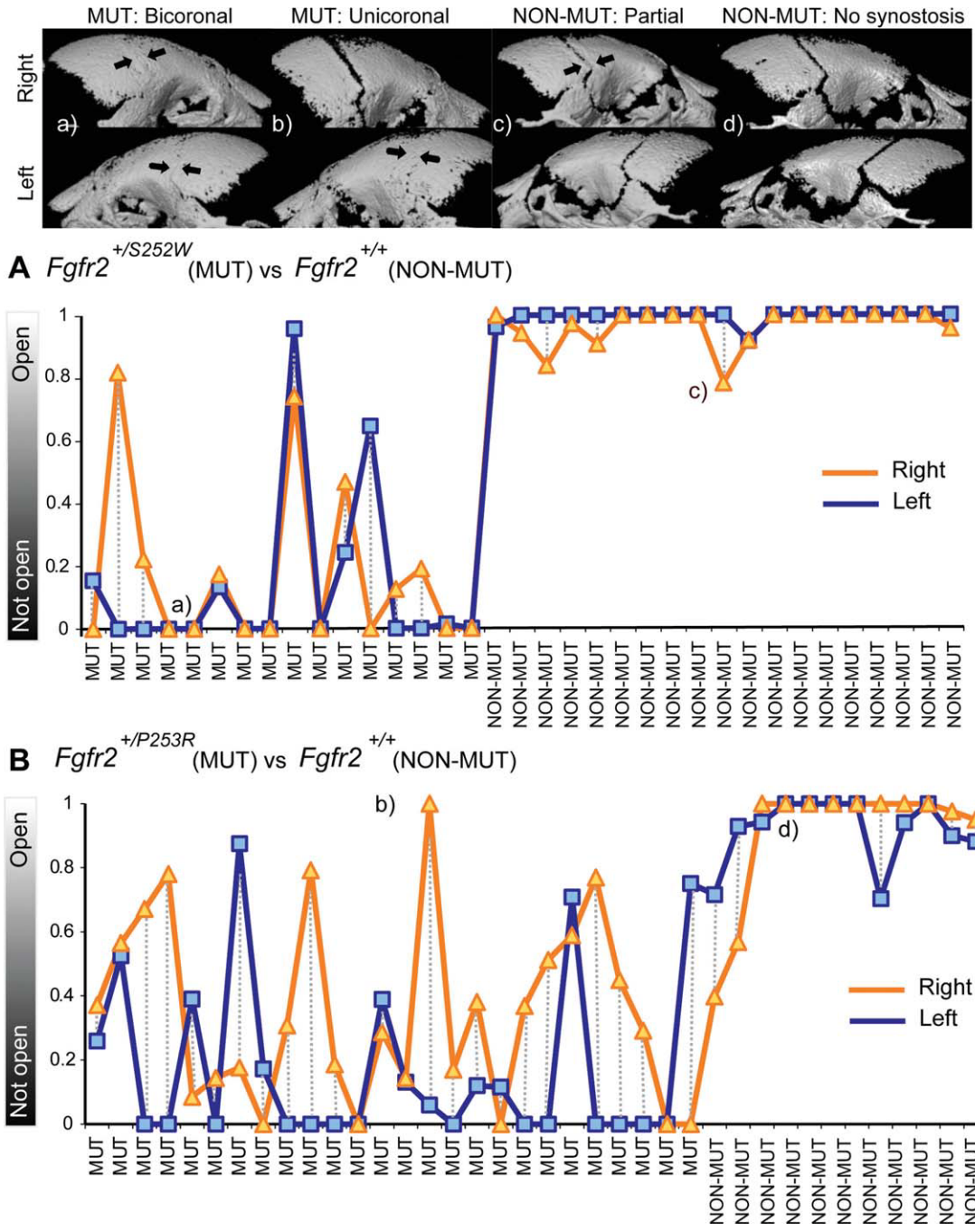
Fig. 6. Quantitative variation in patterns of coronal suture patency in Apert mouse models. **Top:** Right and left lateral views of the 3D reconstructions of μCT images of the skulls of the following specimens: (**a**) *Fgfr2*$^{+/S252W}$ mutant mouse with bicoronal synostosis, (**b**) *Fgfr2*$^{+/P253R}$ mutant mouse with unicoronal synostosis, (**c**) a non-mutant littermate of the S252W model showing partial fusion at the right coronal suture, and (**d**) a non-mutant littermate of the P253R model with completely open coronal sutures. Non-patent sutures are indicated with black arrows. The four individuals (a, b, c, d) shown at top are indicated on the graphs. **Bottom:** Scatter plots showing quantification of coronal suture patency on the right (orange line, triangles) and left sides (blue line, squares) of the coronal suture of each individual plotted in the horizontal axis. Vertical axes represent degree of patency (0 completely non-patent, 1 completely patent). **A:** Comparison of *Fgfr2*$^{+/S252W}$ mice (MUT) and non-mutant littermates (NON-MUT). **B:** Comparison of *Fgfr2*$^{+/P253R}$ mice (MUT) and non-mutant littermates (NON-MUT).

and left coronal sutures. Kruskal-Wallis and Median tests confirm that the difference among mean ranks of suture closure in mutant and non-mutant mice is statistically significant ($Z_{252MUT/NO-MUT} = 5.62$, $P < 0.001$; $Z_{253MUT/NO-MUT} = 4.04$, $P < 0.001$). Coronal suture indices estimated for *Fgfr2*$^{+/S252W}$ mice tend towards the extremes, indicating coronal sutures that are either completely open or completely not open, while intermediate index values predominate among *Fgfr2*$^{+/P253R}$ mice. These differences in suture closure patterns between *Fgfr2*$^{+/S252W}$ and *Fgfr2*$^{+/P253R}$ were not statistically significant ($Z_{252MUT-253MUT} = 1.39$, $P = 0.97$).

Developmental Dynamics

Apert Syndrome *Fgfr2*^{+/S252W} and *Fgfr2*^{+/P253R} Skull Phenotype Is Not Strongly Correlated With Coronal Suture Patency

To directly test the relationship between indices of coronal suture patency and craniofacial dysmorphology associated with Apert syndrome, we applied multivariate regression analysis of cranial shape as defined by the Procrustes coordinates of the whole skull configuration of landmarks on the quantitative scores of suture patency for the right and left sides. If the relationship between suture patency and skull dysmorphology is strong, we expect cranial shape and coronal patency to be highly correlated. Although correlation can never imply causality, a lack of correlation strongly suggests that there is little or no relationship between the two traits (cranial shape and suture patency) at least at P0, suggesting that one trait cannot occur as the consequence of the other. Results showed low, but significant regression coefficients between cranial shape and quantitative scores of suture patency (Left side: $r^2 = 0.15$; $P < 0.001$; Right side: $r^2 = 0.19$; $P < 0.001$) (Fig. 7). Scatter plots of the regression results further show that *Fgfr2*$^{+/S252W}$ and *Fgfr2*$^{+/P253R}$ mice do not cluster on the basis of shape according to the degree to which either coronal suture is open or in the process of fusing (Fig. 7). For instance, specimens in which no area of the right or left suture could be considered patent (i.e., value of 0 on the horizontal axis) are distributed over most of the range of shape variation of the sample (represented by the vertical axis). Importantly, specimens at the far negative end of the distribution are always *Fgfr2*$^{+/S252W}$ mutants indicating a lack of patency of the right and left coronal sutures (Fig. 7).

DISCUSSION

Enormous progress has been made in identifying the association of various mutations with the production of craniosynostosis. Still, a thoughtful consideration underscores that we are no closer to correlating genotype and phenotype in the FGFR-related cra-

niosynostosis syndromes. Previous research has detailed the direct effect of these Apert syndrome mutations on processes of osteogenic cell migration, differentiation, and proliferation with much of the more detailed work focusing on osteogenic cells of the bony fronts of the frontal and parietal bones and the cells of the intervening sutures (Wang et al., 2005, 2010). It is clear that tissues other than bone are affected by these two mutations (Wang et al., 2005, 2010; Aldridge et al., 2010). Here we provide a detailed analysis of global and local skull dysmorphogenesis that is a direct consequence of two related mutations and identify skull locations that should be targeted for more detailed analyses of cell and molecular processes.

Fgfr2$^{+/S252W}$ and *Fgfr2*$^{+/P253R}$ Mice: Overall Similarities, Local Differences

We found statistically significant differences between mice carrying the FGFR2 mutations and their non-mutant littermates, but the skulls of the two mutant models are not different from one another in shape. Skulls of *Fgfr2*$^{+/S252W}$ and *Fgfr2*$^{+/P253R}$ mice are smaller than those of non-mutant littermates, and show the characteristic brachycephaly and midfacial hypoplasia described in individuals with Apert syndrome (Cohen and MacLean, 2000; Du et al., 2010; Wang et al., 2010). Coronal suture patency is highly variable on both the left and right sides (Figs. 5 and 6). Contrary to expectations, the cranial vault shape configuration did not provide the greatest separation among groups (Figs. 3A and S2A) and in both FGFR2 mutant mouse models, craniofacial morphology at P0 is only weakly correlated with coronal suture patency (Fig. 7). Increased variation of calvarial suture closure, as well as independence of skull dysmorphology and coronal suture closure patterns, were also detected in the mouse model for Muenke craniosynostosis syndrome (Twigg et al., 2009), and in those experiments background genes appeared to have a significant effect on suture patency.

Shape differences of the greatest magnitude between Apert syndrome *Fgfr2*$^{+/S252W}$ and *Fgfr2*$^{+/P253R}$ mutant mice are localized to the posterior hard palate (Fig. 4). This suggests that the localized effects of the two mutations are different, potentially targeting different cell populations, different cellular processes, or different temporally sensitive processes or events. The morphological difference between the two mutant models is not generalized, but instead highly localized.

Facial Dysmorphology Is a Primary Locus of Craniofacial Dysmorphology in Apert Syndrome Mice

Our findings do not support a developmental interpretation in which craniosynostosis of the coronal suture is the primary source of skull dysmorphology in Apert syndrome mice at P0. The explicit testing of the relationship between suture patency and skull dysmorphology demonstrates that premature suture closure occurs within a developing head in which many tissues are directly affected by genetic mutations. Developmental integration of these tissues will also influence phenotypic outcomes. Facial and palatal traits, including the invariant fusion of two facial sutures in mutant mice, contribute significantly to the difference between mutant and non-mutant groups and to the discrimination between *Fgfr2*$^{+/S252W}$ from *Fgfr2*$^{+/P253R}$ mutant mice at P0 (Figs. 3C, 4, and S2C). This suggests that facial shape is fundamentally affected by the FGFR2 mutations, contributing to several malformations that play a key role defining the Apert syndrome craniofacial phenotype.

Patterns of coronal suture closure are altered in *Fgfr2*$^{+/S252W}$ and *Fgfr2*$^{+/P253R}$ mutant mice in comparison to their non-mutant littermates at P0 at the morphological (Table 1, Fig. 6) and the molecular level (Wang et al., 2005, 2010). Suture closure may progress with age in these Apert syndrome mouse models and this may, in part, explain the more severe craniofacial phenotypes observed in adult mice (Wang et al., 2005; Du
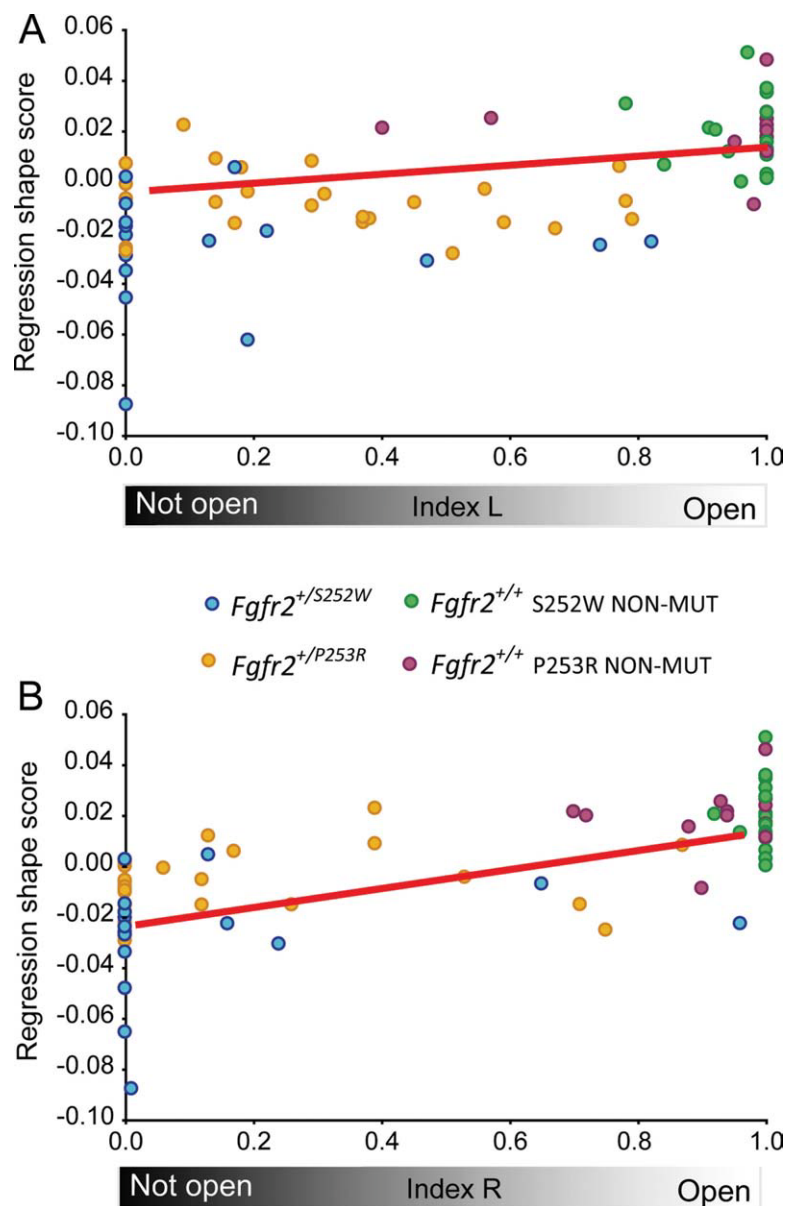
Fig. 7. Regression of cranial shape on quantitative scoring of coronal suture patency. Scatter plot of cranial shape on quantitative scores of left (**A**) and right (**B**) coronal suture patency. Red line shows linear regression. Regression shape score on vertical axis indicates the range of shape variation of the sample. Index L and R on horizontal axes represent degree of patency of left and right coronal suture (0 completely non-patent, 1 completely patent).

Fgfr2$^{+/P253R}$ mutant mice. The observed differences in severity of cranial phenotypes in these mouse models correspond with what has been observed in human cases of Apert syndrome. Comparative analyses have shown that the face is relatively more affected in patients carrying the S252W mutation (Slaney et al., 1996; Lajeunie et al., 1999; von Gernet et al., 2000; Wang et al., 2010). Differential loss of ligand specificity of FGFR2 S252W and P253R mutations may explain some of the reported morphological differences (Yu et al., 2000). It has been suggested, for example, that the P253R mutation will increase the affinity of the FGFR2 receptors toward any FGF, whereas the S252W mutation elicits a more selective response and only enhances the affinity of FGFR2 toward a limited subset of FGFs (Ibrahimi et al., 2001). Shape differences among Apert mouse models may also be due to differences in location and timing of expression of the FGF receptors and their ligands.

One interpretation of our morphometric analyses predicts differential alteration of FGF/FGFR signaling in the two Apert mouse models local to the posterior portions of the palate, the same region where altered expression of FGFR2 has been reported in Crouzon mouse models (Snyder-Warwick et al., 2010). Snyder-Warwick et al. (2010) demonstrated the complex mechanisms through which FGF/FGFR signaling participates in palatogenesis, and showed that a gain-of-function mutation in FGFR2 results in a loss-of-function phenotype: cleft palate. The genes harboring mutations implicated in craniosynostosis (e.g., FGFR1-3) are expressed in many tissues, play fundamental and widespread roles in development, and interact with a multitude of signaling pathways (Ornitz and Itoh, 2001). It may be that each mutation has differential effects, possibly due to variations in expression of FGF/FGFR signaling and complex interactions of downstream signaling cascades (Slaney et al., 1996; Wang et al., 2010). However, these differences in expression profiles may show complex interactions and a level of stochasticity that defies detection by current methods.

et al., 2010). However, as facial dysmorphology is already established at P0 and is more severe than dysmorphology of the cranial vault, facial features cannot be considered as alterations resulting from calvarial suture fusion. Our results do not provide information regarding the temporal sequence of the appearance of facial or neurocranial traits, or any information about cause and effect. Given the widespread expression patterns of fibroblast growth factors and their receptors in development, it is

likely that both regions are fundamentally affected by globally and locally altered FGF/FGFR signaling processes and that very few features can be considered as simply the secondary consequence of other primary abnormalities.

Despite overall similarity in craniofacial phenotypes of *Fgfr2*$^{+/S252W}$ and *Fgfr2*$^{+/P253R}$ mutant mice, facial shape analysis indicates that quantitatively, the *Fgfr2*$^{+/S252W}$ facial phenotype differs more from their non-mutant littermates relative to

Conclusions

Considering the complex scenario involved in normal and abnormal cranial development, it is unlikely that a single mutation will only affect one tissue (i.e., suture mesenchyme, osteogenic fronts of opposing bone) and that a single anomaly will trigger the cascade of diverse craniofacial dysmorphologies associated with craniosynostosis. Recent research has demonstrated that differential expression of FGF receptors and their ligands is not only associated with premature calvarial suture closure, but is also correlated with variation and severity of midface retrusion and cleft palate in craniosynostosis syndromes (Wilke et al., 1997; Bachler and Neubuser, 2001; Britto et al., 2002; Rice et al., 2004; Nie et al., 2006; Cunningham et al., 2007; Szabo-Rogers et al., 2008; Snyder-Warwick et al., 2010). Aldridge et al. (2010) demonstrated that brain dysmorphology, which is also primarily affected in $Fgfr2^{+/S252W}$ and $Fgfr2^{+/P253R}$ mice at P0, is not strongly correlated with craniosynostosis.

Focus on the nature of sutures and their premature closure in craniosynostosis syndromes has provided detailed knowledge about sutures as growth centers (Opperman, 2000; Rice, 2008), the importance of cell lineage in cranial vault bone development and suture patterning (Jiang et al., 2002; Quarto et al., 2009), the critical balance of proliferation and differentiation of osteogenic cells in the developing suture (Chen et al., 2003), and the importance of tissue boundaries in suture definition and in craniosynostosis (Merrill et al., 2006; Ting et al., 2009; Roybal et al., 2010), but the broader picture of the effects of these mutations on craniofacial development and dysmorphogenesis remains obscure. Our findings show that FGFR2 mutations influence not only the coronal suture, but facial sutures and bones of the cranial vault, cranial base, face, and palate, along with the brain (Aldridge et al., 2010). We propose that shared phenogenetic processes, such as regional differentiation by dynamic inductive signaling and repetitive patterning by quantitative interactions (Weiss and Buchanan, 2004; Weiss, 2005), affect-

ing osseous, central nervous system, and other tissues during morphogenesis of the head, underlie not only premature suture closure, but additional cranial anomalies in Apert syndrome. Further morphometric analyses of animals at earlier embryonic and later postnatal ages are in progress and will inform our future molecular and histological studies. Comparisons among $Fgfr2^{+/S252W}$ and $Fgfr2^{+/P253R}$ mice and their non-mutant littermates will allow us to establish more accurately the sequence of events that leads to Apert syndrome craniofacial phenotypes as well as the complex interactions involved in normal craniofacial development.

EXPERIMENTAL PROCEDURES

Generation of Targeting Construct and Apert FGFR2 Mouse Models

Our sample consisted of $Fgfr2^{+/S252W}$ and $Fgfr2^{+/P253R}$ Apert syndrome mouse models and their non-mutant littermates (see Table 1 for sample sizes) generated at Johns Hopkins Medical Institutions and Mount Sinai Medical Center (Wang et al., 2005, 2010). Both knock-in mouse models have been back-crossed onto the same genetic C57BL/6J background more than ten generations, allowing direct comparison between models. Newborn mice (P0) were euthanized before weaning by inhalation anesthetics and fixed in 4% paraformaldehyde. Gestation time was 19.0 ± 0.5 days. Genotyping of tail DNA by PCR was performed to distinguish mutant from non-mutant littermates (Wang et al., 2005, 2010). Mouse litters were produced in compliance with animal welfare guidelines approved by the Johns Hopkins University and the Mount Sinai School of Medicine Animal Care and Use Committees.

µCT Imaging Protocols of Mouse Skull at P0

High-resolution micro-computed tomography (µCT) images were acquired by the Center for Quantitative Imaging at Pennsylvania State University (www.cqi.psu.edu) using the HD-600 OMNI-X high-resolution

X-ray computed tomography system (Bio-Imaging Research Inc, Lincolnshire, IL). Pixel sizes range from 0.015 to 0.020 mm, and slice thickness from 0.016 to 0.025 mm. Image data were reconstructed on a 1,024 × 1,024 pixel grid as a 16-bit TIFF but reduced to 8 bit for image analysis.

Landmark Data Collection and Shape Analysis

Each specimen was digitized twice by the same observer and measurement error was minimized by averaging the coordinates of the two trials (Richtsmeier et al., 1995; Aldridge et al., 2005). To ascertain the accuracy and reproducibility of landmark placement, intraobserver error (i.e., absolute difference between the two trials) was checked for every landmark. If landmark placement differed by more than 0.05 mm, the landmark was remeasured. If this level of accuracy was not met for a specific landmark, it was excluded from analysis. For precise landmark definitions, see Supp. Table S1 and visit our website http://getahead.psu.edu/LandmarkNewVersion/P0mouseskull_updated_applet.html.

Procrustes Analysis

To extract shape information, a global skull, as well as regional configurations of landmarks representing the cranial vault, cranial base, and face, were superimposed separately after a Generalized Procrustes Analysis using MorphoJ (Klingenberg, 2008). This procedure minimizes the effects of scale, translation, and rotation (Rohlf and Slice, 1990), but does not eliminate the allometric shape variation that is related to size. In order to test how allometry affected our samples, we computed a regression of shape (represented by Procrustes coordinates) on centroid size (Drake and Klingenberg, 2008). Centroid size is computed as the square root of the summed distances between each landmark coordinate and the centroid of the landmark configuration (Dryden and Mardia, 1998). To analyze shape variation within and among groups, we computed Principal Components Analyses (PCA) for each landmark configuration. PCA performs a

coordinate rotation that aligns the transformed axes (PCs) with the directions of maximum variation.

Euclidean Distance Matrix Analysis

To statistically determine shape differences between groups, we used EDMA, Euclidean Distance Matrix Analysis (Lele and Richtsmeier, 1995, 2001). EDMA converts 3D landmark data into a matrix of all possible linear distances between unique landmark pairs and tests for statistical significance of differences between shapes using non-parametric confidence intervals (Lele and Richtsmeier, 1995, 2001). We tested for morphological differences in each mutant group as compared to its non-mutant littermates, and we tested for differences in the mutant/non-mutant contrasts in the two mouse models for Apert syndrome.

Confidence intervals were used to statistically evaluate the similarity of groups of linear distances defined for the face, cranial base, and cranial vault using a non-parametric bootstrapping procedure (Lele and Richtsmeier, 2001). Use of these subsets in the evaluation of regional shape differences ensures that the sample size exceeds the number of landmarks considered, a prerequisite for statistical testing. For each region, an average form is estimated using the linear distance data, and differences in three-dimensional size and shape are statistically compared as a matrix of ratios of all like linear distances in the two samples. The null hypothesis for each comparison is that there is no difference in shape between groups (or no difference in shape contrasts). In our specific application, the null hypothesis of similarity between mutant and non-mutant mice within each Apert syndrome model was evaluated using 100,000 bootstrapped group assignments made randomly and with replacement from the non-mutant sample.

Statistical tests for differences in shape of specific linear distances are evaluated by an alternate non-parametric bootstrapping procedure (Lele and Richtsmeier, 1995). For each linear distance, a ratio between the average values of that distance for each group is computed and confidence intervals

for the null hypothesis of similarity in shape differences are estimated from 100,000 pseudo-samples generated from the data using a non-parametric bootstrapping algorithm. For each linear distance, the null hypothesis is rejected if the 90% confidence interval produced from the bootstrapping method does not include 1.0. Rejection of the null hypothesis enables localization of differences to specific landmarks and linear distances (Lele and Richtsmeier, 1995, 2001).

Analysis of differences in the effects of the two FGFR2 mutations required a statistical analysis of the mutant/non-mutant contrasts in the Apert syndrome $Fgfr2^{+/S252W}$ mouse model compared to the $Fgfr2^{+/P253R}$ model. Within each model, shape difference for each anatomical region is estimated as the relative change in the lengths of linear distances between mutant and non-mutant mice using the methods described above. Differences in the effects of the two mutations are estimated as a ratio of the defined difference metrics for the two Apert syndrome mouse models. The contrast between $Fgfr2^{+/S252W}$ mutant and non-mutant mice estimated for each linear distance was entered as the numerator while the contrast between $Fgfr2^{+/P253R}$ mutant and non-mutant mice for the corresponding measure was the denominator. As in the study of shape differences within each sample, a non-parametric statistical test was used to determine whether patterns of mutant/non-mutant contrasts differed between $Fgfr2^{+/S252W}$ and $Fgfr2^{+/P253R}$ mice using non-parametric confidence intervals (100,000 bootstrapped steps) for groups of landmarks that defined an anatomical region ($\alpha = 0.10$) (Richtsmeier and Lele, 1993). EDMA analyses were performed using WinEDMA (Cole, 2002).

Patterns of Suture Patency

Patency of calvarial and facial sutures was scored using the 3D μCT reconstructions. We defined the coronal suture as the curved edge between the frontal and the parietal bones spanning from landmark 41 to landmark 45 on the left side, and from landmark 42 to landmark 46 on the right side (Supp. Fig. S1). We have focused on the patent rather than on

the fused state of the coronal suture because the coronal suture is a beveled suture and the isosurfaces may confound overlapping suture fronts with fused sutures.

For each specimen, right and left coronal sutures were scored qualitatively as open (O) when more than 75% of the length of the suture is completely open; partial (P) when more than 25% but less than 75% of the length of the suture is open; and fused (F) when more than 75% of the length of the suture is not open. A corresponding quantitative measure was obtained for each suture as an index of the open length of the suture divided by its total length. Given the discrete nature of patency of the right and left zygomatic-maxillary and premaxilla-maxillary facial sutures, we were able to assign a qualitative score of either open (O) or closed (F).

To test for significant differences in patterns of suture patency between mutant and non-mutant mice within a model, and among mutants of the two models, non-parametric Kruskal-Wallis and Median tests were conducted using Statistica 6.0 (Statsoft, Inc.). The null hypothesis is that the different samples are drawn from the same distribution or from distributions with the same median.

Finally, to assess the correlation between cranial shape and patterns of coronal suture patency, we performed multivariate regressions of shape on the right and left quantitative score of coronal suture patency using MorphoJ (Klingenberg, 2008). The statistical significance of the regressions was tested with permutation tests against the null hypothesis of statistical independence (Dryden and Mardia, 1998; Drake and Klingenberg, 2008).

REFERENCES

Aldridge K, Boyadjiew S, Capone G, DeLeon V, Richtsmeier JT. 2005. Precision and error of three-dimensional phenotypic measures acquired from 3dMD

photogrammetric images. Amer J Med Genet 138:247–253.

Aldridge K, Hill CA, Austin JR, Percival C, Martinez-Abadias N, Neuberger T, Wang Y, Jabs EW, Richtsmeier JT. 2010. Brain phenotypes in two FGFR2 mouse models for Apert syndrome. Dev Dyn 239:987–997.

Bachler M, Neubuser A. 2001. Expression of members of the Fgf family and their receptors during midfacial development. Mech Dev 100:313–316.

Britto JA, Evans RD, Hayward RD, Jones BM. 2002. Toward pathogenesis of Apert cleft palate: FGF, FGFR, and TGF beta genes are differentially expressed in sequential stages of human palatal shelf fusion. Cleft Palate Craniofac J 39:332–340.

Chen L, Li D, Li C, Engel A, Deng CX. 2003. A Ser252Trp [corrected] substitution in mouse fibroblast growth factor receptor 2 (Fgfr2) results in craniosynostosis. Bone 33:169–178.

Cheverud J. 1995. Morphological integration in the Saddle-Back Tamarin (*Saguinus fuscicollis*) cranium. Am Naturalist 145:63–89.

Cohen MM Jr. 1986. Craniosynostosis: diagnosis, evaluation, and management. New York: Raven Press.

Cohen M Jr. 2000. Apert syndrome. In: Cohen M Jr, MacLean R, editors. Craniosynostosis: diagnosis, evaluation, and management. New York: Oxford University Press. p 316–353.

Cohen MM Jr, MacLean R, editors. 2000. Craniosynostosis: diagnosis, evaluation, and management. New York: Oxford University Press.

Cohen MM Jr. 1993. Sutural biology and the correlates of craniosynostosis. Am J Med Genet 47:581–616.

Cohen MM Jr, Kreiborg S. 1996. A clinical study of the craniofacial features in Apert syndrome. Int J Oral Maxillofac Surg 25:45–53.

Cohen MM Jr, Kreiborg S, Lammer EJ, Cordero JF, Mastroiacovo P, Erickson JD, Roeper P, Martinez-Frias ML. 1992. Birth prevalence study of the Apert syndrome. Am J Med Genet 42:655–659.

Cole T III. 2002. WinEDMA Version 1.0.1 beta. Windows-Based Software for Euclidean Distance Matrix Analysis.

Cunningham ML, Seto ML, Ratisoontorn C, Heike CL, Hing AV. 2007. Syndromic craniosynostosis: from history to hydrogen bonds. Orthod Craniofac Res 10:67–81.

Drake AG, Klingenberg CP. 2008. The pace of morphological change: historical transformation of skull shape in St Bernard dogs. Proc Biol Sci 275:71–76.

Dryden I, Mardia K. 1998. Statistical shape analysis. Chichester: John Wiley and Sons.

Du X, Weng T, Sun Q, Su N, Chen Z, Qi H, Jin M, Yin L, He Q, Chen L. 2010. Dynamic morphological changes in the skulls of mice mimicking human Apert syndrome resulting from gain-of-function mutation of FGFR2 (P253R). J Anat 217:97–105.

Ford-Perriss M, Abud H, Murphy M. 2001. Fibroblast growth factors in the developing central nervous system. Clin Exp Pharmacol Physiol 28:493–503.

Hajihosseini MK. 2008. Fibroblast growth factor signaling in cranial suture development and pathogenesis. In: Rice D, editor. Craniofacial sutures: development, disease and treatment. Front Oral Biol. Basel: Karger. p 160–177.

Holmes G, Rothschild G, Roy UB, Deng CX, Mansukhani A, Basilico C. 2009. Early onset of craniosynostosis in an Apert mouse model reveals critical features of this pathology. Dev Biol 328: 273–284.

Ibrahimi OA, Eliseenkova AV, Plotnikov AN, Yu K, Ornitz DM, Mohammadi M. 2001. Structural basis for fibroblast growth factor receptor 2 activation in Apert syndrome. Proc Natl Acad Sci USA 98:7182–7187.

Inatani M, Irie F, Plump AS, Tessier-Lavigne M, Yamaguchi Y. 2003. Mammalian brain morphogenesis and midline axon guidance require heparan sulfate. Science 302:1044–1046.

Jiang X, Iseki S, Maxson RE, Sucov HM, Morriss-Kay GM. 2002. Tissue origins and interactions in the mammalian skull vault. Dev Biol 241:106–116.

Klingenberg C. 2008. MorphoJ. In: Faculty of Life Sciences, University of Manchester, UK: http://www.flywings.org.uk/MorphoJ_page.htm.

Lajeunie E, Cameron R, El Ghouzzi V, de Parseval N, Journeau P, Gonzales M, Delezoide AL, Bonaventure J, Le Merrer M, Renier D. 1999. Clinical variability in patients with Apert's syndrome. J Neurosurg 90:443–447.

Lele S, Richtsmeier J. 1995. Euclidean distance matrix analysis: confidence intervals for form and growth differences. Am J Phys Anthropol 98:73–86.

Lele S, Richtsmeier JT. 2001. An invariant approach to the statistical analysis of shapes. London: Chapman and Hall/CRC Press. 308 p.

Marie PJ, Kaabeche K, Guenou H. 2008. Roles of FGFR2 and Twist in human craniosynostosis: insights from genetic mutations in cranial osteoblasts In: Rice D, editor. Craniofacial sutures. development, disease and treatment. Front Oral Biol. Basel: Karger. p 144–159.

Merrill AE, Bochukova EG, Brugger SM, Ishii M, Pilz DT, Wall SA, Lyons KM, Wilkie AO, Maxson RE Jr. 2006. Cell mixing at a neural crest-mesoderm boundary and deficient ephrin-Eph signaling in the pathogenesis of craniosynostosis. Hum Mol Genet 15:1319–1328.

Nie X, Luukko K, Kettunen P. 2006. FGF signalling in craniofacial development and developmental disorders. Oral Dis 12:102–111.

Opperman L. 2000. Cranial sutures as intramembranous bone growth sites. Dev Dyn 219:472–485.

Ornitz DM, Itoh N. 2001. Fibroblast growth factors. Genome Biol 2:1–12.

Ornitz DM, Marie PJ. 2002. FGF signaling pathways in endochondral and intramembranous bone development and human genetic disease. Genes Dev 16:1446–1465.

Park W, Meyers G, Li X, Theda C, Day D, SJ Orlow, Jones M, Jabs E. 1995a. Novel FGFR2 mutations in Crouzon and Jackson-Weiss syndromes show allelic heterogeneity and phenotypic variability. Hum Mol Genet 4:1229–1233.

Park WJ, Theda C, Maestri NE, Meyers GA, Fryburg JS, Dufresne C, Cohen MM Jr, Jabs EW. 1995b. Analysis of phenotypic features and FGFR2 mutations in Apert syndrome. Am J Hum Genet 57:321–328.

Plotnikov AN, Hubbard SR, Schlessinger J, Mohammadi M. 2000. Crystal structures of two FGF-FGFR complexes reveal the determinants of ligand-receptor specificity. Cell 101:413–424.

Quarto N, Wan DC, Kwan MD, Panetta NJ, Li S, Longaker MT. 2010. Origin Matters: Differences in Embryonic Tissue Origin and Wnt Signaling Determine the Osteogenic Potential and Healing Capacity of Frontal and Parietal Calvarial Bones. J Bone Miner Res 25:1680–1694.

Reyment R, Blackith R, Campbell N. 1984. Multivariate morphometrics. London: Academic Press. 233 p.

Rice D. 2008. Developmental anatomy of craniofacial sutures. In: Rice D, editor. Craniofacial sutures: development, disease and treatment. Front Oral Biol. Basel: Karger. p 1–21.

Rice R, Spencer-Dene B, Connor EC, Gritli-Linde A, McMahon AP, Dickson C, Thesleff I, Rice DP. 2004. Disruption of Fgf10/Fgfr2b-coordinated epithelial-mesenchymal interactions causes cleft palate. J Clin Invest 113:1692–1700.

Richtsmeier JT. 2002. Cranial vault morphology and growth in craniosynostoses. In: Mooney MP, Siegel MI, editors. Understanding craniofacial anomalies: the etiopathogenesis of craniosynostoses and facial clefting. New York: Wiley-Liss. p 321–341.

Richtsmeier JT, Lele S. 1993. A coordinate-free approach to the analysis of growth patterns: models and theoretical considerations. Biol Rev Camb Phil Soc 68:381–411.

Richtsmeier J, Paik C, Elfert P, Cole TI, Dahlman H. 1995. Precision, repeatability, and validation of the localization of cranial landmarks using computed tomography scans. Cleft Palate Craniofac J 32:217–227.

Rohlf FJ, Slice D. 1990. Extensions of the Procrustes method for the optimal superimposition of landmarks. Syst Zool 39:40–59.

Roybal PG, Wu NL, Sun J, Ting MC, Schafer CA, Maxson RE. 2010. Inactivation of Msx1 and Msx2 in neural crest reveals an unexpected role in suppressing heterotopic bone formation in the head. Dev Biol 343:28–39.

Schuller AC, Ahmed Z, Ladbury JE. 2008. Extracellular point mutations in FGFR2 result in elevated ERK1/2 activation and perturbation of neuronal differentiation. Biochem J 410:205–211.

Slaney SF, Oldridge M, Hurst JA, Moriss-Kay GM, Hall CM, Poole MD, Wilkie AO. 1996. Differential effects of FGFR2 mutations on syndactyly and cleft palate in Apert syndrome. Am J Hum Genet 58:923–932.

Snyder-Warwick AK, Perlyn CA, Pan J, Yu K, Zhang L, Ornitz DM. 2010. Analysis of a gain-of-function FGFR2 Crouzon mutation provides evidence of loss of function activity in the etiology of cleft palate. Proc Natl Acad Sci USA 107:2515–2520.

Sperber GH, Sperber SM, Guttman GD. 2010 Craniofacial embryogenetics and development, 2nd ed. Shelton, CT: People's Medical Publishing House.

Szabo-Rogers HL, Geetha-Loganathan P, Nimmagadda S, Fu KK, Richman JM. 2008. FGF signals from the nasal pit are necessary for normal facial morphogenesis. Dev Biol 318:289–302.

Ting MC, Wu NL, Roybal PG, Sun J, Liu L, Yen Y, Maxson RE Jr. 2009. EphA4 as an effector of Twist1 in the guidance of osteogenic precursor cells during calvarial bone growth and in craniosynostosis. Development 136:855–864.

Turner N, Grose R. 2010. Fibroblast growth factor signaling: from development to cancer. Nat Rev Cancer 10:116–129.

Twigg SR, Healy C, Babbs C, Sharpe JA, Wood WG, Sharpe PT, Morriss-Kay GM, Wilkie AO. 2009. Skeletal analysis of the Fgfr3(P244R) mouse, a genetic model for the Muenke craniosynostosis syndrome. Dev Dyn 238:331–342.

von Gernet S, Golla A, Ehrenfels Y, Schuffenhauer S, Fairley JD. 2000. Genotype-phenotype analysis in Apert syndrome suggests opposite effects of the two recurrent mutations on syndactyly and outcome of craniofacial surgery. Clin Genet 57:137–139.

Wang Y, Xiao R, Yang F, Karim BO, Iacovelli AJ, Cai J, Lerner CP, Richtsmeier JT, Leszl JM, Hill CA, Yu K, Ornitz DM, Elisseeff J, Huso DL, Jabs EW. 2005. Abnormalities in cartilage and bone development in the Apert syndrome FGFR2 (+/S252W) mouse. Development 132:3537–3548.

Wang Y, Sun M, Uhlhorn VL, Zhou X, Peter I, Martinez-Abadias N, Hill CA, Percival CJ, Richtsmeier JT, Huso DL, Jabs EW. 2010. Activation of p38 MAPK pathway in the skull abnormalities of Apert syndrome Fgfr2+P253R mice. BMC Dev Biol 10:22.

Weiss K, Buchanan A. 2004. Genetics and the logic of evolution. New York: Wiley-Liss. 541 p.

Weiss KM. 2005. The phenogenetic logic of life. Nat Rev Genet 6:36–45.

Wilke TA, Gubbels S, Schwartz J, Richman JM. 1997. Expression of fibroblast growth factor receptors (FGFR1, FGFR2, FGFR3) in the developing head and face. Dev Dyn 210:41–52.

Wilkie AO, Slaney SF, Oldridge M, Poole MD, Ashworth GJ, Hockley AD, Hayward RD, David DJ, Pulleyn LJ, Rutland P, Rutland P, Malcolm S, Winter RM, Reardon W. 1995. Apert syndrome results from localized mutations of FGFR2 and is allelic with Crouzon syndrome. Nat Genet 9:165–172.

Yu K, Ornitz DM. 2001. Uncoupling fibroblast growth factor receptor 2 ligand binding specificity leads to Apert syndrome-like phenotypes. Proc Natl Acad Sci USA 98:3641–3643.

Yu K, Herr AB, Waksman G, Ornitz DM. 2000. Loss of fibroblast growth factor receptor 2 ligand-binding specificity in Apert syndrome. Proc Natl Acad Sci USA 97:14536–14541.

Yu K, Xu J, Liu Z, Sosic D, Shao J, Olson EN, Towler DA, Ornitz DM. 2003. Conditional inactivation of FGF receptor 2 reveals an essential role for FGF signaling in the regulation of osteoblast function and bone growth. Development 130:3063–3074.